Finite Element Analysis of an Ultralight Aircraft

T.V. Baughn* and P.F. Packman†
Southern Methodist University, Dallas, Texas

A finite element analysis was conducted to determine the structural integrity of a high-wing cable-supported ultralight aircraft. A simple, symmetrical, half-structure macromodel was analyzed and subjected to level flight loading and two-wheel-landing loading conditions. Flexural and bending stiffness for the supported and unsupported wing were also determined. A preliminary damage tolerance analysis was conducted in which selected cable elements and wing compression struts were removed, the redistributed loads calculated, and possible aircraft flight configurations examined. The model can generate all cable loads, displacement of each structural node (for each loading condition), generate displacement plots, and locate potential highly stressed regions.

Introduction

A POWERED ultralight aircraft is described by the Federal Aviation Administration as weighing less than 254 lb empty, carrying less than 5 U.S. gal of fuel, and operating at a maximum speed of 55 knots and a maximum power-off stall speed not to exceed 24 knots. Ultralight aircraft, as a group, are designed primarily for recreational flying of distances of not more than 100 miles from a home base. However, several recent models have been developed to include aerobatic flying and have been considered by the military for front-line observation aircraft.

The types of ultralights available to the public are diverse, ranging from enclosed cabin structures to high-wing frame structures and power hang gliders. The powerplants can be single or twin engine, pusher or tractor. The landing gear can be equipped for water, snow, or land.

The choice of what type of ultralight design to model was simplified when an initial survey showed that, of 74 designs reviewed, 55 were high-wing pusher type.[1,2] A cable-supported high-wing pusher was finally chosen due to the high percentage of aircraft of this type built and sold. The structure chosen was considered typical of a majority of ultralights. The airloads carried by the wing are transferred to the main frame primarily via tension flying cables. The ground-air-ground loads are transferred from the landing gear to the frame and to the wings via tension landing cables.

Many of these aircraft are evolutionary designs rather than designed completely from scratch. A complete structural analysis of these aircraft is not found in open literature. For this reason it was decided to develop an analysis that could be applied to simple ultralight structures. The model could then be extended to consider more sophisticated structural configurations and analysis procedures.

The purpose of this study was to evaluate the potential high-stress regions of the structure under normal flight conditions and to extend the analysis to a damage tolerance analysis that would determine what alternate structure would take the load in the event of in-flight structural failure of preselected components. Many ultralight structures are designed as portable and are to be partially disassembled and reassembled at the flying site. It is not too difficult to consider a scenario in which a cable or attachment is poorly reassembled or loosely connected.

Received Feb. 19, 1985; presented as Paper 85-0616 at the AIAA/ASME/ASCE/AHS 26th Structures, Structural Dynamics and Materials Conference, Orlando, FL, April 15-17, 1985; revision received Aug. 27, 1985.

*Associate Professor, Department of Civil and Mechanical Engineering.

†Professor and Chairman, Department of Civil and Mechanical Engineering.

Model Development

The cable-supported ultralight aircraft selected to model has a wingspan of 31 ft, a total length of 16 ft 10 in., and a height of 10 ft 4 in., It is a high-wing aircraft with a conventional landing gear. The wing construction is a basic ladder-type frame made from aluminum tubing. All joints are bolted. The empty weight of the ultralight is 220 lb, with a cargo weight of 232 lb. A sketch of the aircraft is shown in Fig. 1.

The finite element model was developed from measurements taken from a full-scale aircraft. (Plans or drawings were not available.) In addition to the dimensions of the ultralight, the location and type of tubing connections had to be identified. Five basic tubing joints and ten different tubing cross sections were measured.

The tubing material is 6061-T6 aluminum. Typical joints are illustrated in Figs. 2 and 3. Joint stiffness data were not available, and the joints were modeled as infinitely rigid, except for joints as shown in Fig. 3. A joint of this type would be released to rotate about the axis of the bolt. The joints in the airframe have a wide range of stiffness values associated with different tubing assembly procedures. Modeling these joints as rigid does not have a significant impact on the static load distribution. The overly stiff joints will have a slight influence on the deflection pattern generated from the linear, small displacement theory analysis procedure. Joint stiffness valves can be determined by testing the joints themselves or by a detailed finite element model of the individual joints.

The cables on the ultralight are a 7×7 stainless steel cable. The upper cables are called landing wires and are attached to the king post and to the wing spars (see Fig. 1). The cables on the underside of the wing are called flying wires and are connected to fittings located on the fuselage tubing and the wing spars. The fuselage tube is known as the downtube and consists of a double-walled aluminum tube. Each wing has leading- and trailing-edge, inboard and outboard, flying and landing wires. In addition, there is an upper nose cable and two lower nose cables, as well as two upper and lower cables going to the tail section.

Rod elements were used to model the cables. The difference between an actual cable and the rod element was minimized by making the torsional stiffness very small relative to the elastic modulus. All cables are manufactured to a specified length and attached to the aircraft with no pretension. The king post pivots in a fore-aft direction at its attachment point on the

root tube. Eleven cables on the aircraft are attached to the aft end of the king post. When the king post is rotated upward and forward and is snapped into position, pretension is introduced into all the cables. This pretension is small relative to the loads experienced in the cables during flying or landing and was therefore neglected in the analysis.

The finite element studies used an iteration process by which the cable elements were removed from subsequent calculations if the previous run indicated that a cable went into compression. Each load case had to be analyzed separately since it was found that different cables would go into compression under different loading conditions. This method of removing rod elements from the model was chosen for simplicity over the more sophisticated nonlinear gap element. A gap element is a sophisticated element that may be used in connection with a rod element to model a cable so that it would have minimal stiffness and load-carrying capability if the cable were to go into compression. The use of the gap element may have reduced the number of iterations since this process would have been handled internally within the solution procedure. The simpler iteration scheme was selected to enhance the load case learning process.

The upper surface of the wing is covered with a dacron skin. The shape of the upper surface is maintained by wing ribs. During assembly the dacron skin is sleeved onto the leading- and trailing-edge spars. The tension and compression struts are fitted through mounting holes cut into the sleeve at appropriate points on the spar. Torsional loading on a wing panel could possibly put the skin in tension between the compression struts if the distortion of the wing exceeded the total clearance of the mounting holes. It was observed that the torsional distortion present under normal flight conditions was not sufficient to permit load transfer to the skin. The aerodynamic upper skin under flight loading is in chordwise tension, and no lower wing skin surface would be in spanwise tension. Therefore, all bending loads in the wing are carried by the leading- and trailing-edge spars. Hence, the dacron was modeled as nonstructural mass. The engine, propeller, gas, and pilot were also modeled as nonstructural concentrated masses.

A plot of the finite element model is shown in Fig. 4. Note that the aerodynamic control surfaces were not modeled but taken into account in the overall mass of the aircraft. Due to symmetry, only one-half of the aircraft needed to be modeled. Symmetric boundary conditions were imposed along the centerline of the ultralight. The model was run using MSC/NASTRAN and consisted of 103 grid points, 121 CBARS, and 11 CRODS.

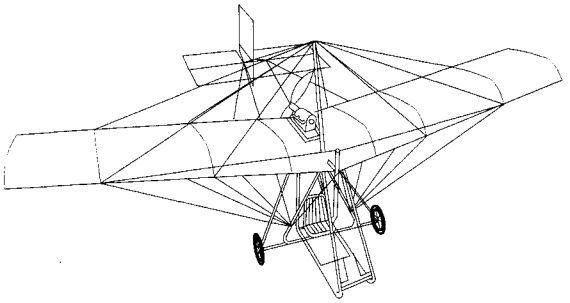

Fig. 1 Sketch of ultralight aircraft.

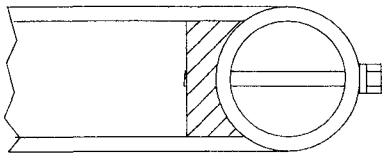

Fig. 2 Compression strut joint.

Loading Configurations

Several loading configurations were simulated for the initial analysis and model verification. These were chosen to reproduce actual service loads the ultralight would encounter under normal flight and landing conditions. Several simulations for the wing structure in bending and torsion were also examined to develop basic design guides. A final series of loading conditions examines the damage tolerance of the cable support system and wing structure. Severe turns and maneuvers were not considered in this paper due to the asymmetric nature of the loads. It is recognized that asymmetric loads can be analyzed using a half-model by adding symmetric and asymmetric load cases. Since different cables will have to be taken out of the analysis, depending upon the boundary conditions and loads, adding these results would not be valid.

Level Flight Loading

The first load case examined is for the aircraft in a straight level flight. The ultralight must be balanced about its center of gravity. The loads acting vertically on the aircraft are the gross lift of the wing, and must equal the weight of the aircraft. The wing lift loads are applied to the wing ribs at 30% of the chord length back of the leading edge and distributed in a manner compatible with high-wing aircraft.[3] A nose-down pitching moment results from the wing lift load being behind the aircraft center of gravity. It is offset by the down lift of the tail. In order to model the aircraft for level flight, the weight of the model was set at 226 lb, one-half of 454 lb total weight. The finite element program calculates the center of gravity and, once the location and magnitude of the wing lift load are known, the magnitude of the required downlift on the tail can be determined. The model can be balanced to represent equilibrium flight conditions by applying the wing lift, the calculated tail-down lift, and gravity loads. When in level flight, the landing cables would carry no tension load and are removed from the model during analysis.

Fig. 3 Cockpit tube joint.

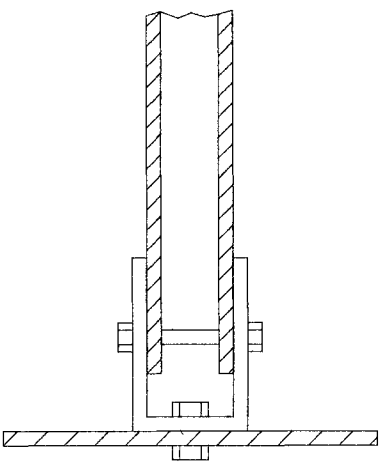

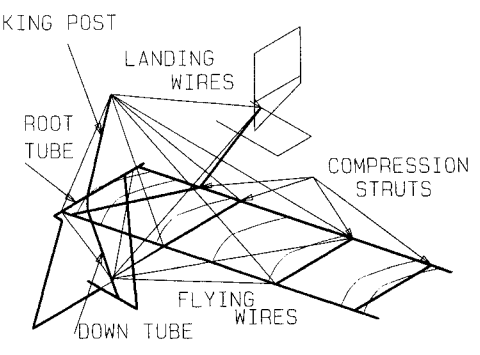

Fig. 4 Undeformed model of ultralight.

The lower cables are the primary load-carrying members during flight. The wing flying wires attach to the cockpit downtube at a single location. The flying wire forces and stresses are listed in Table 1.

As shown in Fig. 4, the upper nose wire connects the front of the root tube to the king post, the upper tail wire connects the king post to the tail, and the lower nose wire connects the front of the root tube to the downtube on the cockpit. The wing flying wires also connect to the same attachment point on the downtube. This single attachment location for the wing and lower nose wire results in the high stress levels in the cockpit downtube. The lower tail wire also connects at this location, but the loads are less than the nose wire loads. The value of the stress in the attachment cannot be reported since the model does not reflect the mechanical complexity of the assembly. The highest stress calculated in the airplane under level flight conditions occurs in the downtube at the downtube cable attachment fittings.

The 7×7 stainless steel flying wires have a yield strength of 70,000 psi. This results in safety factors over 14, assuming a working stress of one-quarter of the yield stress for the highest stressed wire, which is the lower nose wire.

Wing Design Loads

Additional design data were generated for the wing structure. A unit load was placed at the tip of the wing at the leading edge, and the displacement was determined. A similar calculation was made with the load placed at the trailing edge. The displacements were calculated for the wing with and without the cables.

Comparing the wing to a simple cantilever beam fixed at the root, an equivalent flexural stiffness can be determined. The flexural stiffness EI is calculated from the length L of the wing and the deflection Y from the finite element model with a known load F. Hence $EI = -FL^3/3Y$, which is the equivalent flexural stiffness. A similar analysis was conducted to determine the torsional stiffness. The ladder structure of the wing, as in the bending analysis, was fixed at the root, and a unit load was applied to the tip of the wing at the leading edge. The results for both analyses are reported in Table 2.

Landing Loads

The normal landing procedure for an ultralight is to fly the aircraft onto the ground at a safe margin above the stall speed.[2] In the event that the pilot has too fast a sink rate, the airframe would be subjected to an excessive loading into the landing wheels from the ground. This same loading condition could occur if the landing speed is too slow and a wind gust stalls the aircraft. In order to analyze the structure during landing, loads were estimated to be three times the weight (3 g) of the aircraft. The boundary conditions of the model are symmetric, which implies a two-wheel landing. The model was subjected to a 1.5-g load applied at the outboard tip of the axle modeled.

The landing load is simulated using the MSC/NASTRAN inertia relief procedure. In this technique the ultralight is subjected to a loading condition that is not in static equilibrium. The finite element program calculates a rigid body acceleration vector such that the model can be considered to be in

Table 1 Level flight cable forces and stresses

Cable location	Load, lb	Stress, psi
Upper nose wire	174	884
Upper tail wire	48	242
Lower nose wire	243	1238
Inboard leading-edge flying wire	33	170
Inboard trailing-edge flying wire	25	130
Outboard leading-edge flying wire	187	953
Outboard trailing-edge flying wire	103	525

Table 2 Wing flexural and torsional stiffness

Loading point	Cables	Flexural stiffness, psi, $\times 10^6$
Leading edge	Yes	21.9
	No	3.5
Trailing edge	Yes	10.7
	No	2.7
		Torsional stiffness, in.-lb/rad, $\times 10^3$
Leading edge	Yes	12.1
	No	7.3

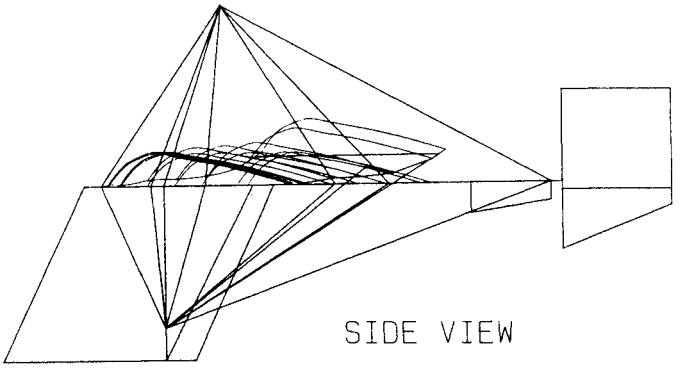

Fig. 5 Level flight deformations.

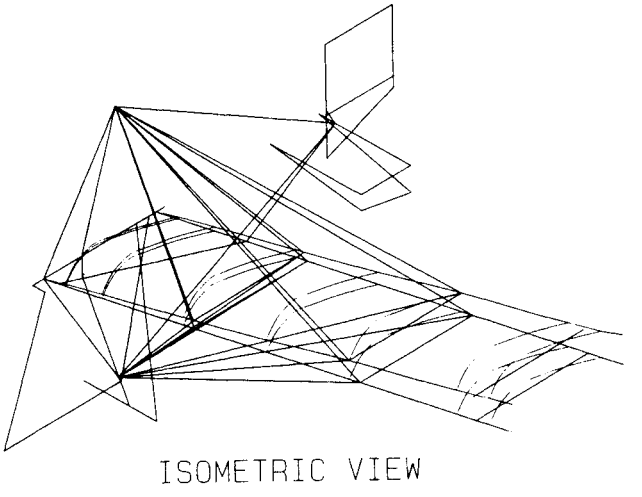

Fig. 6 Level flight deformations.

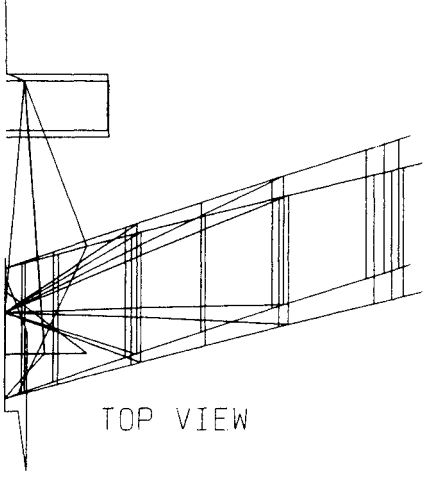

Fig. 7 Landing deformations.

equilibrium with the external forces.[4] A loading of this type approximates the steady-state loads in the airframe during landing but does not include the effects of dynamic transients. In the model analyzed, the upper landing wires will be in tension and are therefore included. The flying wires have been removed. The tip of the wing exhibits a large deflection toward the rear of the aircraft. The magnitude of the deflection is 10.0 in. rearward and 6.2 in. down. These large deflections would introduce some doubt as to the validity of the solution procedure for the 3-*g* load. However, the wing appears to be moving as a rigid body, as shown in Fig. 7. These deflections generate a 3.4-deg rotation of the wing. The highest stress in the wing occurs at the inboard compression strut and is 17,280 psi.

The highest stress during landing was found in the axle. In the model the axle is assumed rigidly attached to the cockpit structure, which would not reflect the actual attachment stiffness. On the ultralight the axle is attached with bungi cords. Therefore, the stress values calculated for the axle most likely represent an upper bound to the true stress value. The model accurately identifies the airplane components that may be subject to failure under 3-*g* landings. i.e., the axle, the inboard compression strut, and the downtube.

Damage Tolerance Analysis

The adaptation of a damage tolerance analysis for standard aircraft structures to an ultralight structure involves three steps. First, an analysis is made of the static strength of critical components. Second, an analysis is made of the residual static strength of the damaged structure to determine what alternate load paths exist and the additional loads that are imposed on the remaining structure. Finally, the analysis is extended to cyclic loading caused by gust loads, the ground-air-ground cycle, and taxi to determine the potential service life of fatigue critical parts. The results presented in this paper represent the first two steps of the damage tolerance analysis procedure. It had generally been assumed that ultralights are immune to fatigue failures because of the low stresses during flight. However, recent experience has indicated that several structural components have failed by fatigue, resulting in loss of control of the aircraft.

From Table 2 it is obvious that the cable system contributes significantly to the flexural and torsional stiffness of the wing structure. The loads in the cables are significantly below the cable-rated working loads. This minimizes the probability of cable failure under normal flight conditions and under the 3-*g* landing conditions, assuming that the cables have not been abused. Hence, the critical flight components would be the cable attachment points. The residual strength analysis simply assumes that preselected cables cannot carry any load and makes no assumptions as to the mode of failure of the cable attachment.

The loads in selected components of the ultralight have been discussed previously. In this section an analysis of the loads in the damaged structure is presented. In addition, an evaluation has been made on the effect of the damage on displacements of the remaining structure, failure modes, and possible flight configuration changes. In certain cases, examination of the surrounding structure shows that it would fail when the stiffening cable is lost.

The damaged structure evaluated is considered to be the loss of flying cables and the loss of wing compression struts. It is obvious that the loss of the nonredundant main structure, i.e., king posts, wing spars, downtubes, or root tube, results in loss of the aircraft. The following damaged configurations were evaluated:

A) Upper nose wire out.
B) Upper tail wire out.
C) Lower nose wire out.
D) Both inboard flying wires out.
E) Outboard leading-edge flying wire out.
F) Outboard trailing-edge flying wire out.
G) Inboard compression strut out.
H) Outboard compression strut out.

Table 3 summarizes the loads in each of the remaining cables for the given damaged condition. The damaged structure is indicated by the particular wire or strut removed; the cable loads are recalculated. If a cable then remaining in the system goes into compression, it is indicated by "Comp."

The least damaging cable "out" configuration is D. The loads in the outboard flying wire increase significantly, but the frame cable loads do not change. One possible failure mode would be longitudinal buckling of the aluminum wing spars due to the greater unsupported length. It was found that the axial load in the leading-edge spar was considerably below the buckling load calculated from a simplified analysis. Local buckling may occur at the stress concentration hole located at the inboard flying wire attachment.

The loss of the outboard flying wires, configurations E (leading edge) and F (trailing edge), does not affect the frame wire loads. If the outboard leading-edge flying wire is lost, the load is transferred to the inboard leading-edge flying wire, with little change in the trailing-edge inboard flying wire. Similarly, in case F, the load is transferred to the inboard trailing-edge cable, with little change in the leading-edge cable loads. Loss of either outboard wire would cause the wing to twist significantly outboard of the last pair of surviving flying wires. The direction of twist depends upon whether the leading- or trailing-edge wire failed. If the remaining wing survived, the aircraft would enter a spin (probably nonrecoverable), resulting in loss of the aircraft.

Loss of frame wires results in a slight increase in the load on the outboard flying wires and a significant redistribution of loads in the inboard flying wires. Upper tail wire out (B) and lower nose wire out (C) produces compression in the inboard trailing-edge flying wire. This indicates a downward motion in this area of the wing, increasing the angle of attack of the wing. The loss of the upper nose wire (A) causes a reverse motion, decreasing the angle of attack. Decreased lift on the wing would result in a roll maneuver.

When the upper tail wire is removed (B), the upper nose wire loses tension. When the upper nose wire is removed, the

Table 3 Damage tolerance loads in flying wires, lb

Cable location	Level flight	A	B	C	D	E	F	G	H
Upper nose	174	Out[a]	2	158	170	173	179	Comp[b]	Comp
Upper tail	48	Comp	Out	43	46	47	49	Comp	Comp
Lower tail	243	62	152	Out	246	202	288	Comp	Comp
Inboard leading edge	33	Comp	53	67	Out	209	21	32	41
Inboard trailing edge	25	13	Comp	Comp	Out	24	135	28	19
Outboard leading edge	187	222	186	176	222	Out	220	187	184
Outboard trailing edge	103	113	115	105	123	142	Out	104	106

[a]Out implies the cable was removed from the analysis;[b] comp implies the cable went into compression in the analysis.

upper tail wire goes into compression. In both cases, the surviving tail structure would be unable to sustain the tail loads. The loss of the tail moment arm would cause an abrupt nose-down for the aircraft.

The loss of the inboard and outboard wing compression struts (G and H) results in loss of tension in all fuselage flying wires, with only slight rearrangement of the loads in the inboard and outboard wing flying wires. The unsupported wing spar will probably buckle in a chordwise direction at the point of the lost compression strut. Loss of either wing compression strut appears to result in a major in-flight breakup of the aircraft.

Conclusions

The MSC/NASTRAN finite element program can easily be adapted to model a typical ultralight structure under a variety of loading configurations. Each commercial model design contains enough differences to make an overall structural analysis unrealistic. The model used in the analysis was symmetric about the longitudinal axis of the aircraft. The airframe loads under asymmetric loading configurations were difficult to evaluate. Thus, a single-wheel-landing configuration was not considered. Each loading configuration must be examined to determine which cables go into compression; the cable is removed from the analysis and then recalculated. This procedure is adequate for the level flight loads. A more detailed model consisting of a full rather than one half aircraft, subject to similar loads with a geometric nonlinear solution procedure and nonlinear gap elements for the cables, would be the next logical step in the structural analysis.

The first two steps in the damage tolerance analysis indicate that, in addition to the king post and downtube structures, the wing compression struts and some fuselage flying wires are flight-critical. The loss of inboard and outboard flying wires in flight may produce nonrecoverable maneuvers. The loss of frame wires redistributes the loads in the remaining flying wires, resulting in twisting of the wing. This change in wing configuration can result in abrupt roll and/or yaw motion. The loss of the upper nose wire results in an abrupt nose-down attitude.

The simplified analysis of the ultralight structure has shown several significant factors. The critical components of the typical ultralight structure are nominally overdesigned. The analysis shows very high static safety factors on the major structural components. These safety factors may be reduced considerably due to the local stress concentrations associated with design details.

References

[1]Drisdale, T. and Hanes, S., *The Ultralight Aviator's Handbook*, Skyflight International, Manhattan Beach, CA, 1982, pp. 28-134.

[2]Markowski, M.A., *Ultralight Aircraft*, Ultralight Publications, Hummelstown, PA, Oct. 1983, pp. 12-220, 255-260.

[3]Markowski, M.A., *Ultralight Flight*, Ultralight Publications, Hummelstown, PA, 1982, pp. 102-130.

[4]Schaeffer, H.G., *MSC/NASTRAN Primer, Static and Normal Modes Analysis*, Wallace Press, Milford, NH, 1982, pp. 309-312.